Aerospace Science and Technology 23 (2012) 439–451

Contents lists available at SciVerse ScienceDirect

Aerospace Science and Technology

www.elsevier.com/locate/aescte

Design and performance characterization of a sub-Newton N_2O monopropellant thruster

Guobiao Cai [a], Wei Sun [a,*], Jie Fang [a], Mao Li [a], Yu Cong [b], Zhe Yang [c]

[a] School of Astronautics, Beihang University, Beijing, 100191, China
[b] Laboratory of Catalysis and New Materials for Aerospace, Dalian Institute of Chemical Physics, Dalian, Liaoning, 116023, China
[c] Chinese Academy of Space Technology, Beijing, 100086, China

ARTICLE INFO

Article history:
Received 3 December 2010
Received in revised form 7 July 2011
Accepted 1 October 2011
Available online 7 October 2011

Keywords:
Nitrous oxide
Monopropellant
Micro-propulsion
Self-pressurization
Preheating

ABSTRACT

This paper describes the research at Beihang University for developing a sub-Newton thruster based on catalytic decomposition of nitrous oxide (N_2O) for fine attitude control of small spacecrafts. The characteristics of the N_2O self-pressurization feeding process as well as the preheating process of a sub-Newton N_2O thruster were studied. Experimental and simulated results indicated that the tank pressure decreases during the N_2O self-pressurization process. The influence on the preheating process of the surface emissivity, the preheating power, the thickness of combustor chamber and the insulation material, were compared. N_2O catalytic decomposition experiments were carried out to evaluate the reaction performance of Iridium impregnated modified alumina catalyst, such as activation temperature and reaction temperature. Successful activation and self-sustaining reaction were achieved at 523 K. It was found that the integral structure of the reactor and the loading factor of the catalyst-bed can influence the reaction effect. Based on further experiments looking for proper catalyst-bed, a thruster with a $\Phi 10$ mm $\times$ 25 mm catalyst-bed was designed and fabricated. The vacuum performance of the thruster at different N_2O flow rates was evaluated using a vacuum experimental system, which consists of a vacuum chamber and a sub-Newton-thrust measuring stand. Static vacuum thrusts ranging from around 140 mN to 970 mN were achieved with the flow rates altering from around 0.1 g/s to 0.6 g/s. The highest specific impulse reached 1640 N s/kg.

1. Introduction

The function of small satellites has been extended by employing formation flying technology [2,9,15,11]. Through partitioning the function of a single large satellite to a number of small satellites, the mission risks and the total cost can be reduced. Micro-propulsion system, defined by Micci and Ketsdever as any propulsion system that is applicable to a micro-spacecraft (mass less than 100 kg) [12], is used for high accuracy station keeping and attitude control of small spacecrafts. It is regarded as a key technology for successful application of micro-satellites. Requirements such as accurate control and high level reliability are often demanded for a micro-propulsion system. In addition, small size of a micro-satellite will bring many new constraints such as volume and power limits to the design of a micro-propulsion system. Thus, propulsion systems onboard micro-satellites should be subject to both common and unique requirements [19].

Micro-propulsion systems can generally be divided into two categories according to fabrication technology [5,6,13,14]: one is scaling down the conventional propulsion systems by conventional fabrication technology; and the other is the design and fabrication based on the MEMS fabrication technology. The MEMS technology is considered to be the next generation propulsion mode; however they are still far from extensive application at present. Conventional propulsion technology remains the primary choice. Although conventional propulsion modes work well in large satellites, they are confronted with many problems when applied to micro-propulsion [24]. For example, low specific impulse performance of cold gas thrusters will limit the maneuver range of micro-satellites; hydrazine-based mono-propellant systems which rely on toxic and flammable propellants will increase the hazard and cost in ground handling; efficiency of bipropellant propulsion systems will be very low when scaled down and their complex structures are unfit for micro-satellites; solid rocket motors are unable to be restarted thus unsuitable for accurate control requirements; electrostatic and electromagnetic propulsion systems usually have high demand on power supply that cannot be supported by power systems onboard micro-satellites.

Therefore, considerable research and development are still required to find new approaches to support micro-propulsion, one of which is to develop new non-toxic mono-propellant to replace the current hydrazine-based monopropellant. Nitrous oxide (N_2O)

* Corresponding author.
E-mail address: buaasw@163.com (W. Sun).

1270-9638/$ – see front matter
doi:10.1016/j.ast.2011.10.003

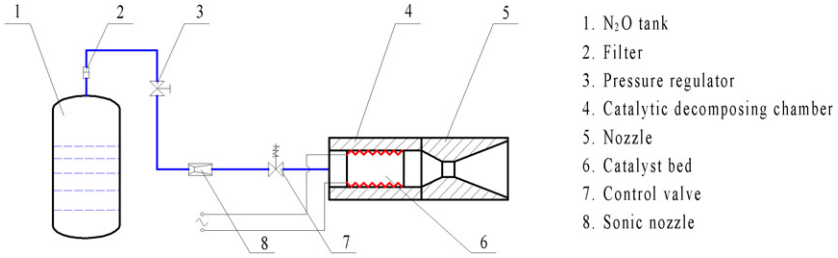

Fig. 1. Sketch of an N_2O monopropellant propulsion system.

is considered to have great potency for providing micro-propulsion [24]. It is non-toxic to human beings and is stable at normal conditions, which will greatly reduce the risk and save the cost in ground handling. The decomposition reaction of N_2O can generate large amounts of heat, which will enhance the reaction temperature to around 1900 K and enable the decomposition reaction to be self-sustaining. The decomposition products of N_2O are a mixture of N_2 and O_2. Therefore, it is a human-friendly and environment-friendly propellant. As a liquefied gas, N_2O is often stored in liquid phase with a high vapor pressure at room temperature. Its high vapor pressure can be used for self-pressurization supply of the N_2O propellant. That will simplify the propellant supply system. In addition, it is compatible with many common structural metals such as stainless steel, aluminum, copper, etc. Because of its unique properties, N_2O can be employed in cold-gas, monopropellant, and bipropellant thrusters [24,4,18,1,22].

Thanks to its low cost and little hazard in handling, propulsion systems using N_2O as the propellant have drawn great interests of universities. The University of Surrey has made great efforts to verify the feasibility of using N_2O as a monopropellant by analyzing properties of N_2O and comparing it with conventional and alternative propellants [24]. The researchers have tested more than fifty different catalysts for N_2O catalytic decomposition, and finally achieved repeatable, self-sustaining decomposition of N_2O with different catalysts. An activation temperature as low as 250 °C and a decomposition temperature in excess of 1500 °C were recorded [22]. They have found N_2O decomposition inside the decomposer is a flow-controlled process and the start-up transient for N_2O decomposition is shorter for higher energy input [23] and also summarized the characteristic of the N_2O decomposition process in a catalyst-bed [20]. However, most of the researches at Surrey were obtained for non-choked flow at ambient pressure, therefore the researches at Tsinghua University aimed at the hot firing of choked N_2O flow. Based on Surrey's researches, researchers at Tsinghua have successfully reduced the size of N_2O decomposer as well as the start-up transient from 15 min to 52 s [25,26]. In addition, they have developed a model for the simulation of a nitrous oxide (N_2O) monopropellant thruster operation [21]. Researchers at the Stanford University have designed and tested an N_2O monopropellant gas generator for propulsion and power applications [10,16]. Different from the researches at Surrey and Tsinghua, Stanford's gas generator was operated at higher N_2O mass flow rates ranging from 0.9 g/s to 2.3 g/s. High efficiency of the characteristic velocity under steady state was demonstrated with loading factors up to 15 kg/(m^2 s) in the gas generator. They also studied the effects of lean CH_4/N_2O mixtures on the reaction initiation.

Although a considerable amount of researches have been conducted, none of the former researches have investigated the relation between the specific impulse performance of a thruster and the N_2O decomposition process directly. Both the researches at Surrey and Tsinghua focused on the N_2O decomposition process. Although research at Stanford has evaluated the C* efficiency of the thruster and predicted the thrust, it has not given any guidance for the design of an N_2O monopropellant thruster. In the current paper, theoretical analysis and experiments were carried out to find the relation between N_2O catalytic decomposition and specific impulse performance of an N_2O monopropellant thruster. Based on the theoretical analysis and preliminary experiments, a sub-Newton N_2O monopropellant thruster was designed and fabricated. Vacuum-thrust measuring tests were carried out to evaluate the actual specific impulse performance of the thruster. Basic design guidelines for a sub-Newton N_2O monopropellant thruster were discussed. Furthermore, numerical simulation on the N_2O self-pressurization feeding process and the preheating process of the sub-Newton N_2O monopropellant thruster were also presented as two important issues for application of N_2O monopropellant thruster.

Table 1
Configuration of a conical nozzle.

Parameter	Value
Chamber diameter, mm	8
Throat diameter, mm	0.85
Converging angle of nozzle, degree	60
Diverging angle of nozzle, degree	30
Expansion ratio of nozzle	100

2. System scheme and performance prediction

A schematic illustration of an N_2O monopropellant propulsion system is shown in Fig. 1. Prior to operation, the catalyst-bed is preheated to a designated temperature. The initial temperature of the catalyst-bed depends on performance of the catalyst, which has resulted in different startup temperatures in many previous researches. When the catalyst-bed reaches the designated temperature, the preheating power is turn off and the control valve is opened. N_2O gas is fed into the catalyst-bed and N_2O decomposition reaction will be activated. Self-sustaining reaction is achieved when the heat released by decomposition reaction equals the heat lost to the environment. Thrust is produced when the decomposition products eject out of the nozzle.

For the purpose of performance prediction, preliminary numerical simulation was conducted to study the inner-nozzle flow field of an N_2O monopropellant thruster. A conical nozzle was employed as shown in Table 1. Based on thermodynamic analysis, the composition of gaseous mixture at the nozzle inlet is assigned 36.4% O_2 and 63.6% N_2 in mass fraction with an N_2O adiabatic decomposition temperature of 1925 K. Total pressure was assigned 1 MPa at the inlet and 0 Pa at the outlet. No-slip and adiabatic wall boundary conditions were employed on inner wall of nozzle. The governing equations employed were the two-dimensional compressible N-S equations, and the turbulence effect was modeled using the RNG k–ε model. Discretizations for the flow equations, the turbulence kinetic energy equations and the turbulence dissipation-rate equations employed a second-order upwind differencing scheme. A self programming code was employed for the simulation.

Simulated results, including the distributions of the static pressure, temperature, and Mach number of the inner-nozzle flow field,

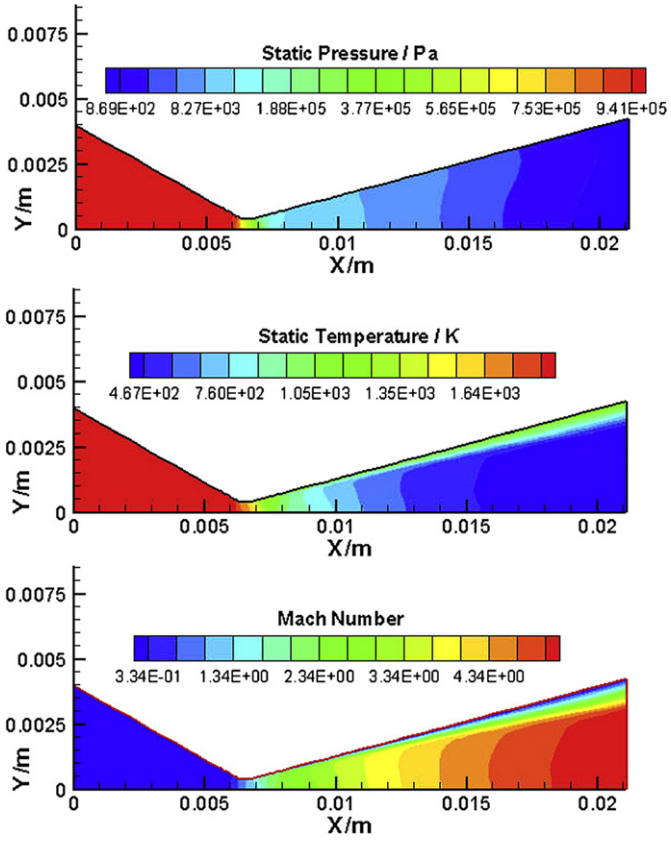

Fig. 2. Simulated results of inner-nozzle flow field.

are shown in Fig. 2. It was found that the viscous effect was obvious at the adjacent wall region, where the boundary layer was thick. This demonstrated the characteristics of the flow under small scale condition and suggested that the influence of friction loss on specific impulse may be more obvious in a small nozzle than in a big one. Integrated results indicated the mass flow rate at the nozzle outlet is about 0.5 g/s and the thrust is 0.95 N, which was close to the targeted vacuum-thrust. The corresponding specific impulse is around 1900 N s/kg.

It should be noted that the above mentioned specific impulse of 1900 N s/kg was obtained under the assumption that the N_2O was completely decomposed in the combustion chamber. However, complete decomposition of N_2O may not be achieved in actual conditions. Thus it is important to study the performance under the condition of N_2O incomplete decomposition and analyze the factors which may affect the performance for further structure design of the thruster and experimental researches. A prediction method using a 1-D isentropic frozen flow model was employed for carrying out qualitative analysis. The vacuum specific impulse can be obtained using the following equation (2.1) [8]:

$$I_s = \mu \frac{C_F}{\Gamma} \sqrt{\frac{R_0 T_f}{M}} \tag{2.1}$$

I_{SP}: specific impulse, N s/kg; μ: coefficient of nozzle loss; C_F: thrust coefficient, N/(Pa m^2); Γ: function of the ratio of specific heat of the mixture; R_0: universal gas constant, 8314 J/(kmol K); T_f: temperature of the gas mixture, K; M: mean molecular weight of the gas mixture, kg/kmol.

The thrust coefficient C_F is a function of the ratio of specific heat of the gas mixture and the nozzle expansion ratio. According to the above equation, the vacuum specific impulse depends on the reaction temperature, the gas composition and the configuration of the nozzle. If the configuration of a nozzle is fixed, the specific impulse of monopropellant thrusters mainly depends on the reaction effect of N_2O decomposition.

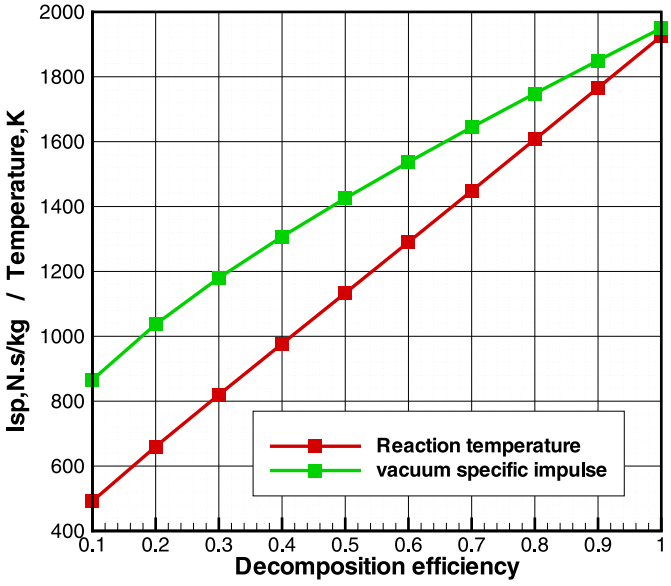

Fig. 3. Temperature and I_{sp} at different N_2O decomposition efficiency.

In order to study the relations between the N_2O decomposition reaction and the specific impulse performance, a variable named as "decomposition efficiency" is employed. It is defined as the percentage of the N_2O that has decomposed in the reaction chamber. Suppose all the decomposed N_2O is transformed to N_2 and O_2 and all the heat released by N_2O decomposition is absorbed by the reaction products, the composition and the temperature of the reaction products will only depend on the decomposition efficiency of the N_2O. This assumption neglects reaction products such as NO and NO_2. However, the influence should be very small due to their small amounts in the gas mixture according to the thermodynamic computation results. Fig. 3 shows the reaction temperature and the vacuum specific impulse at different reaction efficiency.

It is found that the more the N_2O reactant decomposes, the higher the reaction temperature as well as the specific impulse will be. Because the decomposition reaction of N_2O is an exothermic reaction as well as a volume-increase reaction, more heat will be released and more gas products will be produced if more N_2O decomposes, which will bring a higher reaction temperature and a smaller mean molecular weight. According to Eq. (2.1), a higher reaction temperature and a smaller mean molecular weight will bring a higher specific impulse.

3. N_2O self-pressurization feeding for a sub-Newton thruster

N_2O liquefied gas is featured for its high vapor pressure at room temperature. This property can be used to self-pressurize an N_2O tank. However, the tank pressure will decrease during N_2O supply process due to the evaporation of the liquid N_2O in the tank. The pressure drop may influence the stability of the N_2O supply if it exceeds the regulating range of the pressure regulator. In this section, the characteristics of N_2O self-pressurization process of a sub-Newton thruster were studied by numerical simulation and experimental method.

3.1. Modeling for an N_2O tank

An important and difficult step for modeling the self-pressurization process of an N_2O tank is to accurately predict the heat and mass transfer between the liquid N_2O and the gaseous N_2O. A simple equilibrium model assumes that the vapor is always saturated

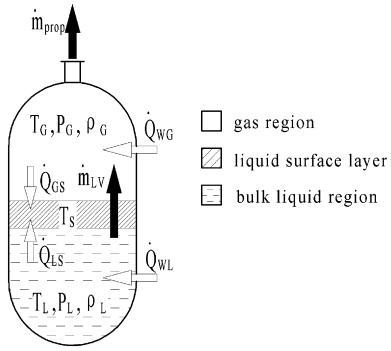

Fig. 4. Tank model for gaseous N_2O feeding.

when there is still liquid in tank, and the temperatures are uniform throughout the two phases and equal to the saturated-liquid temperature [3,17]. This model usually works well when the propellant mass flow rate is very low. However, the gaseous N_2O and the liquid N_2O may not achieve equilibrium and the liquid N_2O may not reach an uniform temperature immediately at moderate to high propellant mass flow rates, e.g. in a hybrid rocket motor using N_2O propellant.

Zilliac and Karabeyoglou have developed a three-region lumped model to study the tank pressurization process of an N_2O hybrid rocket motor [28]. Although the propellant feeding process of an N_2O monopropellant thruster is different from a hybrid rocket motor. Some assumptions in the model can be employed to create a special three-region lumped model for the propulsion system using N_2O mono-propellant. A physical model of an N_2O tank and the nomenclature is shown in Fig. 4 and Table 2. The whole tank is divided into three regions, including a bulk gas region, a liquid surface layer and a bulk liquid region. It is assumed that the actual convection heat-transfer rate between the bulk liquid and the liquid surface layer is much higher than the heat-transfer rate of the common natural convection, thus the heat-transfer coefficient is much higher than the common value correspondingly. The actual heat-transfer coefficient between the bulk liquid and the liquid surface layer can be obtained by multiplying the heat-transfer coefficient of natural convection with an empirical factor which is determined by trial and error comparison. The mass-transfer rate from the liquid region to the gas region, namely the vaporization rate, is proportional to the convection heat-transfer rate between the bulk liquid and the liquid surface layer. Although there is not a convincing explanation and rigid derivation to the empirical factor, it had been verified that the model works well on predicting the correct evaporation rate over a wide range from 0 to 18 kg/m^2 s [28]. The boundary between the N_2O and the inner-wall of the tank is adiabatic. The pressure throughout the tank is uniform. The temperature and composition in the bulk gas region and bulk liquid region are also uniform, although they may be different from each other. The temperature of the liquid surface layer is equal to the saturation temperature under the tank pressure.

The main governing equations, state equation and supplementary equations are listed below.

According to the law of mass conservation, the equations for mass change rate in the bulk gas region and bulk liquid region are:

$$\dot{m}_G = \dot{m}_{LV} - \dot{m}_{prop} \tag{3.1}$$

$$\dot{m}_L = -\dot{m}_{LV} \tag{3.2}$$

The conservation equation of energy for an open system is:

$$\dot{Q}_{in} = \frac{dE}{dt} + \sum \dot{m}_e h_e - \sum \dot{m}_i h_i + \dot{W} \tag{3.3}$$

This equation is applicable to both the bulk liquid region and bulk gas region.

The temperature of the liquid surface layer is equal to the saturation temperature at the tank pressure [7]:

$$T_S = \frac{b}{a - \lg(\frac{P_G}{100000})} - c$$
$$(a = 4.80716087;\ b = 967.819748;\ c = 19.6368887) \tag{3.4}$$

The vaporization rate of the bulk liquid can be calculated with the following equation [28]:

$$\dot{m}_{LV} = -\frac{\dot{Q}_{LS}}{H_{LV}} = -\frac{h_{LSM} A_{LS}(T_L - T_S)}{H_{LV}} = -\frac{f h_{LS} A_{LS}(T_L - T_S)}{H_{LV}}$$
$$(\text{empirical factor } f = 2.1 \times 10^4) \tag{3.5}$$

According to the state equation of real gas [7] and the uniform pressure assumption, the pressure of the bulk gas and bulk liquid are:

$$P_G = \left(\frac{R T_G \rho_G}{44.02 - b\rho_G} - a\left(\frac{\rho_G}{44.02}\right)^2\right) \times 1.01325 \times 10^5$$
$$(R = 0.08206;\ a = 3.782;\ b = 0.04415) \tag{3.6}$$

$$P_L = P_G \tag{3.7}$$

Density equation of the liquid N_2O is [7]:

$$\rho_L = 1000 \times a b^{-(1 - T_L/T_c)^n}$$
$$(a = 0.44927;\ b = 0.27244;\ n = 0.2882;\ T_c = 309.57) \tag{3.8}$$

Total volume of the N_2O tank is:

$$V_G + V_L = \frac{m_G}{\rho_G} + \frac{m_L}{\rho_L} = V_{total} \tag{3.9}$$

Time-dependent state parameters of each region in the physical model can be obtained by working out these equations.

3.2. Derivation and solving for the equations

For the bulk gas control volume, each term in Eq. (3.3) can be written as:

$$\dot{Q}_{in} = -\dot{Q}_{GS} = -h_{GS} A_{GS} \tag{3.10}$$

$$\frac{dE}{dt} = \frac{dU_G}{dt} = \frac{d(H_G - P_G V_G)}{dt} = \frac{d(h_G m_G - P_G V_G)}{dt} \tag{3.11}$$

$$\sum \dot{m}_e h_e = \dot{m}_{prop} h_G \tag{3.12}$$

$$\sum \dot{m}_i h_i = \dot{m}_{LV} h_{G1} = -\dot{m}_L h_{G1} \tag{3.13}$$

$$\dot{W} = \frac{P_G dV_G}{dt} \tag{3.14}$$

where h_G and h_{G1} are the specific enthalpy of gaseous N_2O evaluated at T_G and T_L respectively.

For the bulk liquid control volume, each term in Eq. (3.3) can be written as:

$$\dot{Q}_{in} = -\dot{Q}_{LS} = -h_{LS} A_{LS} \tag{3.15}$$

$$\frac{dE}{dt} = \frac{dU_L}{dt} = \frac{d(H_L - P_L V_L)}{dt} = \frac{d(h_L m_L - P_L V_L)}{dt} \tag{3.16}$$

$$\sum \dot{m}_e h_e = \dot{m}_{LV} h_{G1} \tag{3.17}$$

$$\sum \dot{m}_i h_i = 0 \tag{3.18}$$

$$\dot{W} = \frac{P_L dV_L}{dt} \tag{3.19}$$

Table 2
Nomenclature for the physical model of an N_2O tank.

Symbol	Description	Symbol	Description
T	Temperature, K	ρ	Density, kg/m^3
P	Pressure, Pa	V	Volume, m^3
$\dot{Q}$	Heat-exchange rate, W	$\dot{m}$	Rate of total mass change, kg/s
E	Total internal energy, J	U	Internal energy, J
h	Specific enthalpy, J/kg	H	Total enthalpy, J
Subscript G	Gas region	Subscript L	Bulk liquid region
Subscript S	Liquid surface layer	Subscript W	N_2O tank wall
Subscript ab	Default direction of heat-exchange is from a to b (if not specified) e.g. $\dot{Q}_{LS}$ means heat-exchange rate from the bulk liquid to the liquid surface layer		
$\dot{m}_{LV}$	Vaporization rate of the bulk liquid, kg/s	$\dot{m}_{prop}$	Mass flow rate of propellant, kg/s
$\dot{Q}_{in}$	Net rate of heat comes into the control volume, W	$\dot{m}_e$	Mass flow rates of N_2O leaving the control volume, kg/s
$\dot{m}_i$	Mass flow rate of N_2O entering the control volume, kg/s	h_e	Specific enthalpy of the leaving N_2O, J/kg
h_i	Specific enthalpy of the entering N_2O, J/kg	H_{LV}	Vaporization latent-heat of liquid N_2O at the temperature of the bulk liquid, J/kg
$\dot{W}$	Net rate of work output from the control volume, W	h_{LSM}	Modified heat-transfer coefficient by employing the empirical factor, W/m^2 K
h_{LS}	Heat-transfer coefficient of natural convection between the bulk liquid and liquid surface layer, W/m^2 K	A_{LS}	The interface area of the bulk liquid and the liquid surface layer, m^2
h_{GS}	Heat-transfer coefficient of natural convection between the bulk gas and liquid surface layer, W/m^2 K	A_{GS}	The interface area of the bulk gas and the liquid surface layer, m^2

Substitute Eqs. (3.10)–(3.14) and (3.15)–(3.19) to Eq. (3.3) respectively can obtain the following two equations:

$$m_G\dot{h}_G + h_G\dot{m}_G + h_{G1}\dot{m}_L - \frac{m_G}{\rho_G}\dot{P}_G = -h_{GS}A_{GS} - \dot{m}_{prop}h_G \quad (3.20)$$

$$m_L\dot{h}_L + h_L\dot{m}_L - h_{G1}\dot{m}_L - \frac{m_L}{\rho_L}\dot{P}_L = -h_{LS}A_{LS} \quad (3.21)$$

The heat-transfer coefficient of natural convection between two different regions can be derived from the empirical Nusselt number correlation equations. The specific enthalpy of gaseous N_2O or liquid N_2O is a function of temperature. Due to space limitation, detailed equations for describing heat-transfer coefficient and specific enthalpy are not included in this paper.

There are nine time dependent variables in above mentioned equations namely m_G, m_L, ρ_G, ρ_L, P_G, P_L, T_G, T_L, T_S. Nine independent equations namely (3.1), (3.4)–(3.9), (3.20), (3.21) forms a differential algebra equation set. In the current research, Matlab module for solving differential algebra equation set was used to obtain changes of tank pressure and the other variables over a time interval.

3.3. Simulation and experimental study on the N_2O self-pressurization process

N_2O self-pressurization experiments were carried out to verify the simulation model. Two tanks, with total volumes of 10 L and 3.3 L, were employed in the experiments respectively. The outer-wall of the two tanks was wrapped with insulation materials for thermal isolation from the ambient environment. The initial filling factor of the tank, defined as the average weight of the propellant in unit volume before usage, was altered in the experiments to study the cases under different initial conditions. The mass flow rates of N_2O were kept around 0.7 g/s, since the demand for the N_2O flow rate in a sub-Newton N_2O thruster must be below this value if the specific impulse is above 1500 N s/kg. As a significant parameter that may influence the performance of the propulsion system, tank pressure was measured. The uncertainty of the pressure sensor for tank pressure measuring was ±0.025 MPa.

The comparison of the experimental data and the simulated results with the heat-insulation boundary is shown in Fig. 5. The simulation results agreed well with the experimental results. This indicated the model can be used to predict the N_2O self-pressurization process of a sub-Newton propulsion system. Both

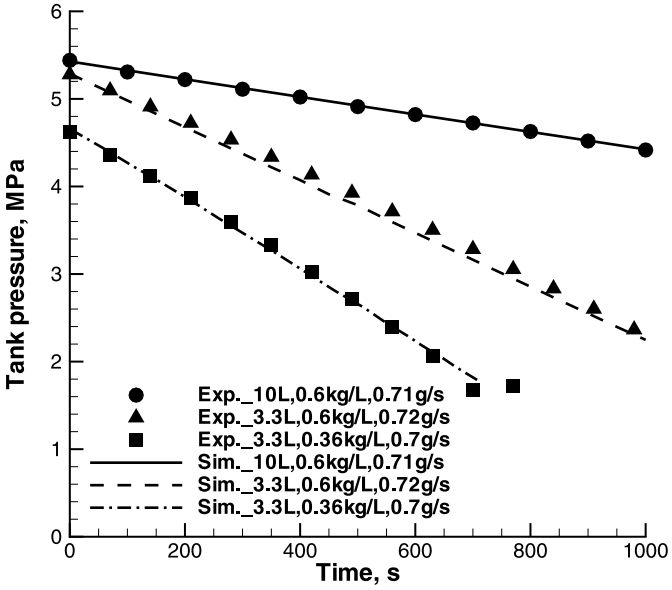

Fig. 5. Experimental and simulated results of N_2O self-pressurization.

experiments and the simulation results indicated there is a faster pressure drop in N_2O tank with a smaller volume or a lower initial filling factor, and a large pressure drop occurred after long-term tank self-pressurization. For example, in the 3.3 L tank with an initial filling factor of 0.36 kg/L, the tank pressure dropped from 4.7 MPa to 1.8 MPa in 700 s after expelling only 41% of the N_2O with a mass flow rate of 0.7 g/s. It suggested that without heat compensation an N_2O tank may not expel all the propellant at a stable mass flow rate due to a large tank pressure drop in late stage of tank self-pressurization process, although the N_2O mass flow rate of a sub-Newton thruster is very low.

4. Preheating process of the N_2O monopropellant thruster

Because the power generated by a power system onboard a small spacecraft is limited, the power can be supplied to the propulsion system is strictly limited. However, the demand for the initial temperature of an N_2O monopropellant thruster usually surpasses 523 K according to the experimental results (described

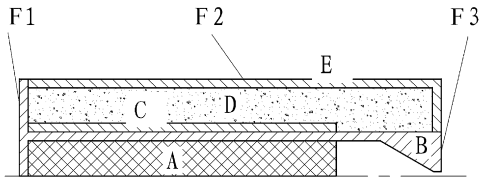

A Catalyst bed D Heat insulation material
B Thruster chamber E Heat insulation sleeve
C Heater F Surface

Fig. 6. Simplified configuration of a monopropellant thruster.

Table 3
Thermodynamic properties of different parts of the thruster.

Part	ρ (kg m^{-3})	C_p (J/kg K)	λ (w/m K)
A	1000	6000	50
B	8700	439	48.1
C	8700	439	48.1
D	60	1067	0.045
E	2000	6000	0.01

Table 4
Simulation cases and results.

No.	P (w)	L_1 (mm)	L_2 (mm)	ε	T_{3600} (K)
1	10	1	15	0.4	653
2	5	1	5	0.1	627
3	3	1	10	0.7	405
4	10	1.5	10	0.1	825
5	5	1.5	15	0.7	445
6	3	1.5	5	0.4	438
7	10	2	5	0.7	658
8	5	2	10	0.4	497
9	3	2	15	0.1	428
K_{i1}	712	562	574	627	
K_{i2}	523	569	576	529	
K_{i3}	424	528	509	503	
R	288	42	67	124	

later) and the previous reports [22,10]. It is higher than the demand of a conventional hydrazine monopropellant thruster. This may become a constraint for the application of the N_2O monopropellant thruster. In this section, numerical simulation was conducted using the commercial software ANSYS to analyze the influence of several factors on the preheating process of the N_2O monopropellant thruster.

4.1. Physical model

The simplified configuration of a monopropellant thruster is shown in Fig. 6. The thermodynamic property of each part is shown in Table 3. ρ, C_p, and λ represent the density, the constant-pressure specific heat, and the coefficient of thermal conductivity of the material respectively. Inner configuration parameters of the thruster have been listed in Table 1. Initial conditions and assumptions were used as follows: The initial temperature of each part in the thruster is 273 K and the environment temperature is 4 K; there only exists radiation heat transfer on surfaces F1, F2 and F3; the thermal contact-resistance between different parts of the thruster is ignored; the preheating power was simulated with a heat generation rate added to the heater part in the model.

4.2. Orthogonal design for simulation cases

In order to compare the influence of different factors on the preheating process and reduce the total number of simulation

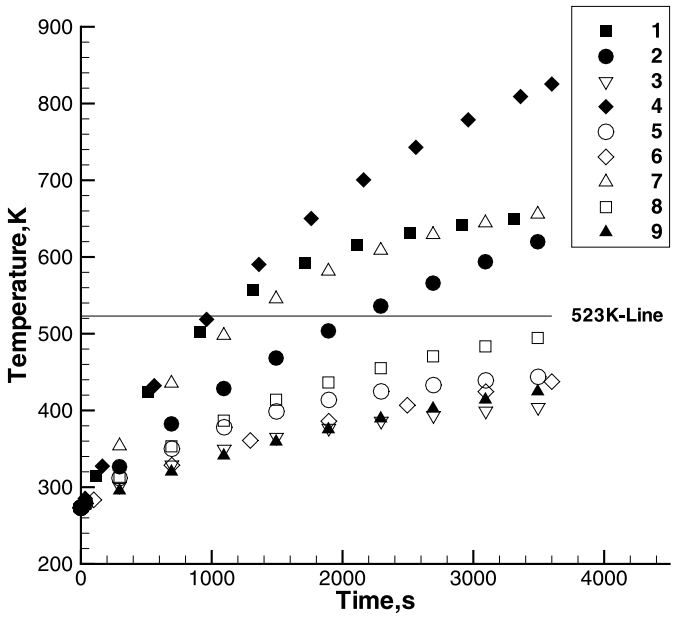

Fig. 7. Temperature curves of the catalyst-bed in different cases.

computation, an L9 orthogonal form [27] as shown in Table 4 was employed to arrange the simulation cases. Four factors, including the preheating power (P), the surface emissivity (ε), the thickness of the combustor chamber (L_1), and the thickness of the thermal insulation material (L_2), were chosen as the influential factors. Each factor was assigned three levels. The central point temperature of the catalyst-bed at 3600 s (T_{3600}) was chosen as the characteristic parameter to evaluate the preheating effect of different thrusters. Parameter K_{ij} in Table 4 represents the average value of the target parameters; subscript i represents the ith factor; subscript j represents the jth level. Parameter R is the difference between the maximum and minimum value of the mean value at different levels of the ith factor. The larger the R value for a factor, the larger the effect the factor has on the process according to the theory for experimental design [27]. It was found that the influence of the preheating power and the surface emissivity were more apparent than the other two factors. Although increasing the preheating power is the most effective way to improve the preheating effect and reduce the preheating duration, reducing the surface emissivity of the thruster may be a more feasible way due to the power limitation in small spacecrafts. This conclusion was applied in the structure design of the N_2O monopropellant thruster later.

Fig. 7 shows the temperature curves of the catalyst-bed in different simulation cases. Only in cases 1, 2, 4, and 7, the temperature can achieve 523 K after 3600 s preheating. It demonstrated the influence of the four factors to the preheating process, because cases 1, 4, and 7 employing the maximum heating power and case 2 using the minimum surface emissivity. It also indicated that although N_2O monopropellant thruster has a higher start-up temperature than the hydrazine monopropellant thruster, its demand can be supported by using preheating power as low as 5 W.

5. Design and performance characterization for a thruster

5.1. Experimental facility

As shown in Fig. 8a, a ground experimental system consisting of an N_2O supply system and a thruster was built. It can be used for studying the N_2O self-pressurization feeding process and conducting catalytic decomposition experiments to evaluate the catalyst

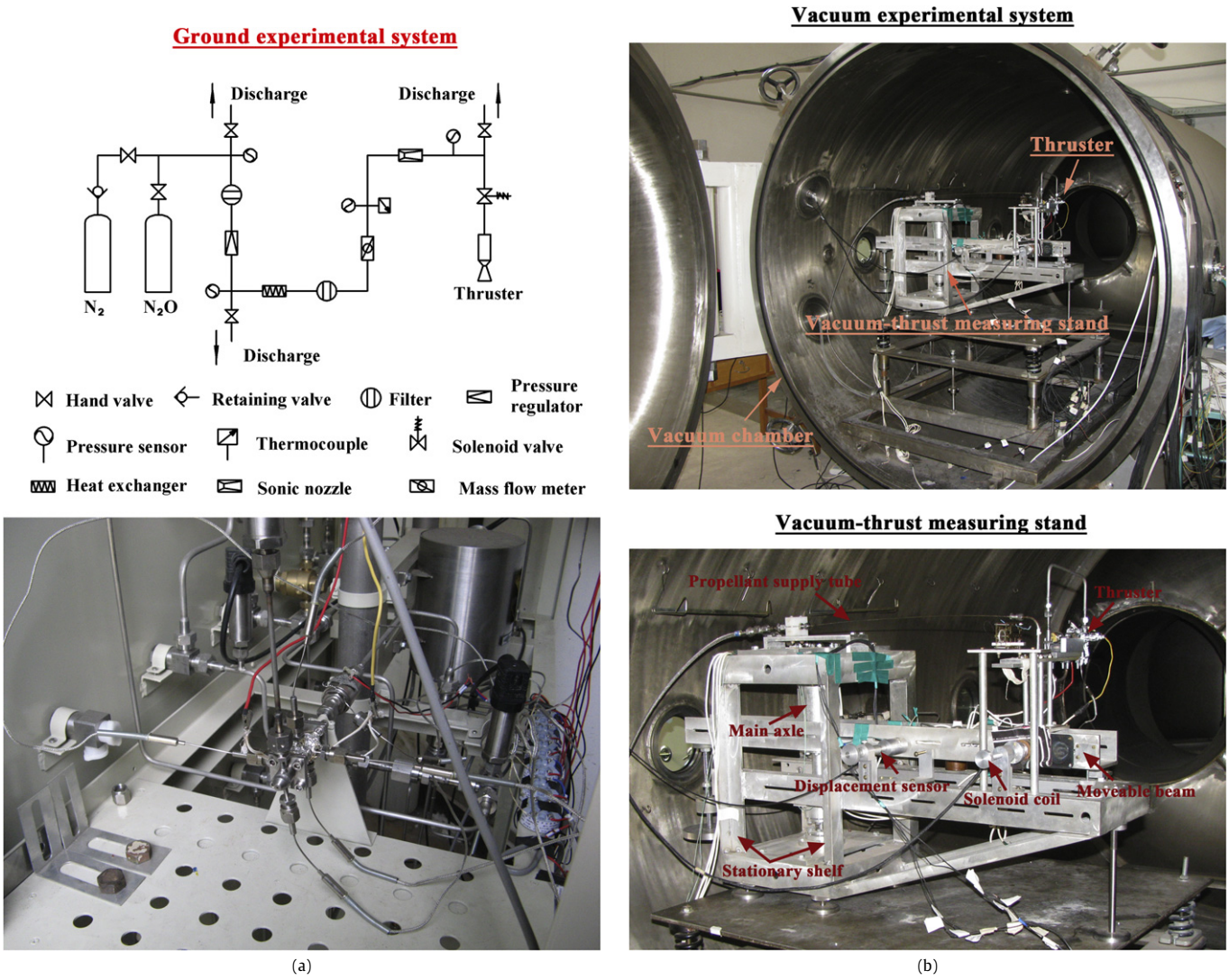

(a) (b)

Fig. 8. (a) Ground experimental system. (b) Vacuum experimental system.

performance. The N_2O supply system uses the vapor pressure of the liquefied N_2O gas to self-pressurize the gas cylinder. It can provide a steady supply of gaseous N_2O for the thruster. The mass flow-rates of N_2O can be altered by adjusting the inlet pressure of a sonic-nozzle or changing the throat diameter of the sonic-nozzle. A heat compensation device was assembled behind the pressure regulator to prevent condensation of N_2O gas, since the temperature of N_2O gas will decrease quickly in the pressure regulator. Several thermocouples, pressure sensors and a mass flow meter were assembled in the system pipelines to monitor the state of the propellant supply system. A solenoid valve was used for a fast on-off control of the N_2O. A thruster (or a reactor) was fixed right behind the solenoid valve. High pressure N_2 gas was employed to purge the pipes before and after N_2O usage.

In order to study the vacuum performance of the N_2O monopropellant thruster, a vacuum experimental system was also employed, which consists of a vacuum chamber and a vacuum-thrust measuring stand. As shown in Fig. 8b, a 1.8 m-diameter and 3.2 m-long vacuum chamber, with a pumping capability of 52 000 L/s, can produce an ultimate vacuum-degree of 5×10^{-5} Pa. The vacuum-thrust measuring stand, which uses electromagnetic force to compensate the thrust produced by the thruster and thus makes the whole system under a state of indifferent equilibrium to eliminate the influence of propellant supply pipe and measuring wires, was adopted for measurement of a steady vacuum-thrust below 1000 mN with an uncertainty of ±2% to the full scale.

5.2. Catalyst preparation

Although the reaction of N_2O decomposition is exothermic, there is a high activation energy-barrier for initiating the reaction. In addition, the decomposition efficiency of N_2O depends on the decomposition rate of the reaction. Thus, a catalyst that can lower the activation energy and increase the decomposition rate for N_2O is necessary for developing an N_2O monopropellant thruster. There are two major challenges in developing an N_2O catalyst: first, the catalyst should effectively reduce the activation temperature and increase the decomposition rate to an applicable range; second, the catalyst should survive and keep its activity at the high temperature for an enough long period.

The catalysts used in the current research were prepared by incipient wetness impregnation of modified alumina with aqueous solution of noble metal soluble compounds, followed by drying at 393 K for 15 hours and subsequent 4 hours calcinations at 773 K or 1473 K. Iridium (Ir) was employed to make the catalysts. The mass fractions of the metal contents in the catalyst were about 15–30%. Iridium impregnated modified alumina catalysts with 17%

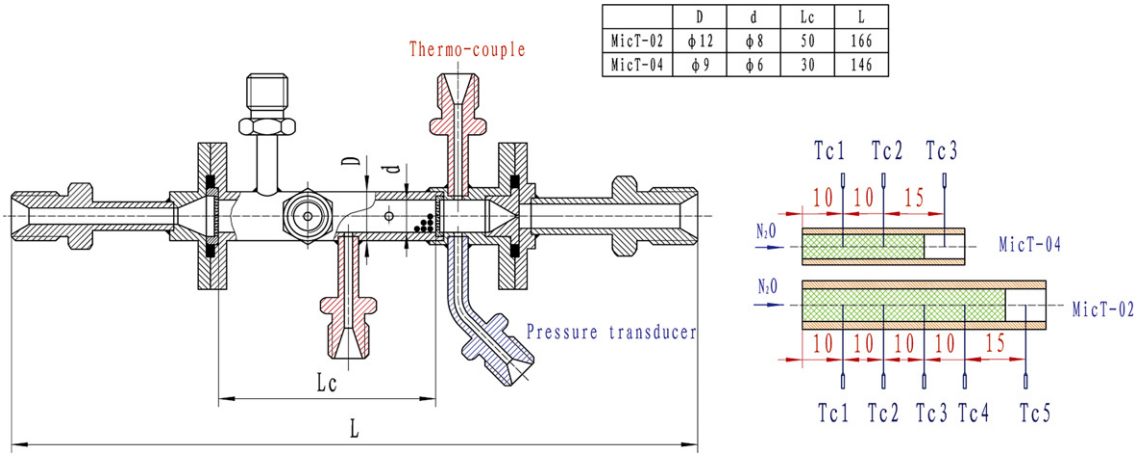

	D	d	Lc	L
MicT-02	ϕ12	ϕ8	50	166
MicT-04	ϕ9	ϕ6	30	146

Fig. 9. Reactors for the 1st round catalytic decomposition experiments.

metal content showed superior performance in N_2O catalytic decomposition experiments and was selected as the catalyst for the current thruster.

5.3. N_2O catalytic decomposition experiments

The reaction of N_2O catalytic decomposition plays an important role for developing an N_2O monopropellant thruster, since it can influence the specific impulse performance. A typical reaction process of N_2O catalytic decomposition in a catalyst-bed can be divided into several continuous phases [20]. Firstly, when the gaseous N_2O just flows into the catalyst-bed, the decomposition reaction rate is very slow because of the low temperature, since the decomposition rate is temperature dependent. The N_2O is then warmed up by heat transferred from the catalyst-bed. This is a "heat-exchange phase". The N_2O decomposition rate will increase gradually and the catalytic decomposition reaction becomes the major reaction in the catalyst-bed. More heat will be released and the temperature of the flow will increase rapidly. This is a "catalytic decomposition phase". If the reaction temperature surpasses 800 °C, thermal decomposition will become the major reaction. This is a "thermal decomposition phase". When most of the N_2O in the flow is decomposed, the temperature of the flow reaches the maximum. After that, the temperature will decrease due to heat dissipation. This is a "heat dissipation phase". The N_2O decomposition reaction is a complicated process that can be influenced by many factors such as catalyst property, catalyst-bed configurations and N_2O mass flow rate. In order to find a proper structure for the sub-Newton thruster, N_2O catalytic decomposition experiments were carried out at first.

Two reactors were employed in the first round experiments. As shown in Fig. 9, the first reactor (MicT-02) has a Φ8 mm × 50 mm cylindrical catalyst-bed; the second reactor (MicT-04) has a Φ6 mm × 30 mm catalyst-bed. Several thermocouples were assembled in the two thrusters with a spacing of 10 mm. The first reactor has four thermocouples embedded in the catalyst-bed and one inserted into the chamber behind the catalyst-bed. The second reactor has two thermocouples embedded in the catalyst-bed and one inserted into the chamber. Reaction activation experiments at different initial catalyst-bed temperatures were carried out at an N_2O mass flow rate of 0.1 g/s. The initial catalyst-bed temperatures were altered from 723 K to 523 K to verify whether a self-sustained reaction can be successfully activated at the corresponding temperature. The temperature curves of the experiments conducted at 523 K in both reactors (shown in Fig. 10a) indicated that the temperatures kept on rising after turning off the heating power, which demonstrated that the N_2O decomposition reaction can be activated at this temperature. It was also found that the reaction temperature in MicT-04 was higher than in MicT-02. This may be caused by the different heat loss rates of reactors. MicT-02 had larger chamber diameter and longer chamber length. Thus the area of heat dissipation on both its inner-wall and outside-wall was larger, which may result in more heat loss. In addition, a larger frame of MicT-02 needs more heat for the same temperature rise due to a higher thermal-capacitance. When increasing the N_2O mass flow rate to 0.13 g/s in MicT-02, there was a notable enhancement of reaction temperature compared to the experimental results at 0.1 g/s in the same reactor (shown in Fig. 10b). It indicated that a higher N_2O mass flow rate may bring a higher reaction temperature. As increasing the mass flow rate or reducing the chamber diameter will bring a higher loading factor, the preliminary experimental results actually indicated that a higher loading factor may result in a higher reaction temperature.

The axial temperature distributions of the two reactors at 100 s are shown in Fig. 11a and Fig. 11b. The thermocouples were numbered according to their locations along the axial direction. In MicT-04 the peak temperature appeared at the second thermocouple, however in MicT-02 it appeared at the first thermocouple. Although the N_2O mass flow rates in the two reactors were the same, the loading factors were different due to their different cross-section areas. Since a peak temperature in the catalyst-bed implied that there was a "major reaction region" nearby, where most of the N_2O decomposed, this phenomenon indicated that the loading factor can influence the reaction effect. In a catalyst-bed with a lower loading factor, the N_2O decomposition reaction can be completed in a shorter distance.

5.4. Catalyst-bed selection

Based on the preliminary N_2O catalytic decomposition experiments, further researches were aimed at enhancing the reaction temperature of N_2O decomposition, for the purpose of acquiring a high specific impulse in the thruster. Since the reaction temperature of N_2O decomposition depends on the configuration of the catalyst-bed as well as the mass flow rate of N_2O. These researches actually focused on looking for a proper catalyst-bed configuration for the thruster at different N_2O mass flow rates. As listed in Table 5, nine different reactors were fabricated. The thickness of the flanges and the chamber wall were designed thinner than the former reactors, since it had been demonstrated that the structure volume may influence the reaction temperature. Two mass flow

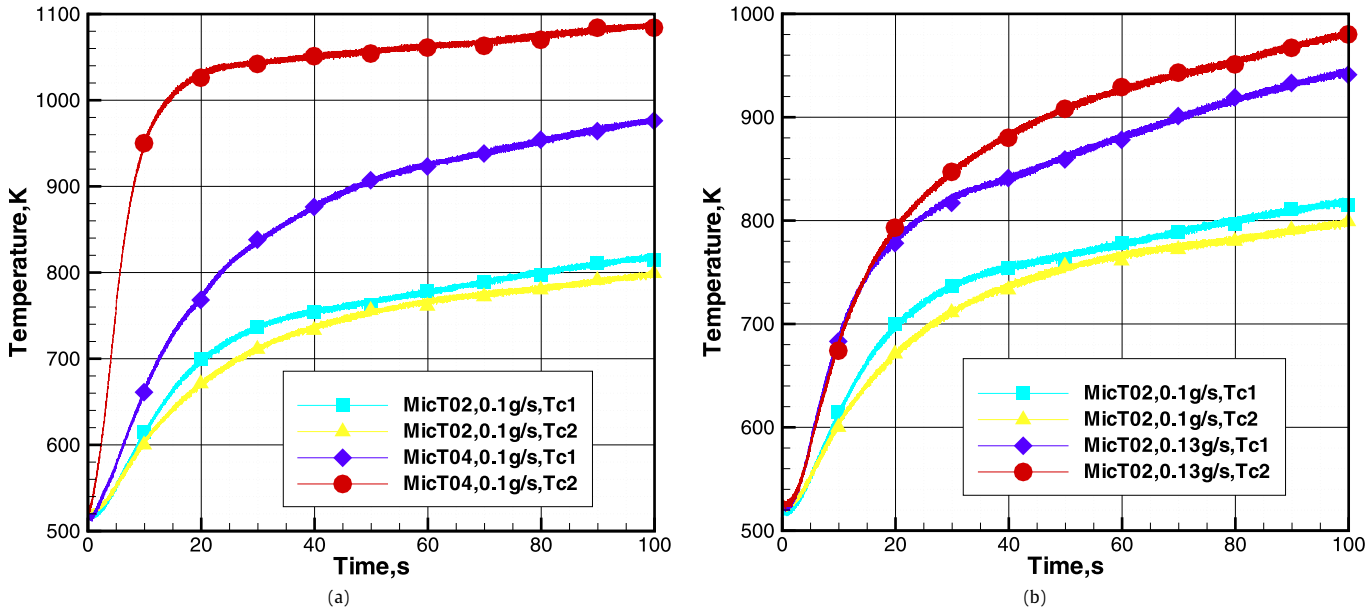

Fig. 10. (a) Reaction temperatures in different reactors at 523 K. (b) Reaction temperatures at different N_2O mass flow rates.

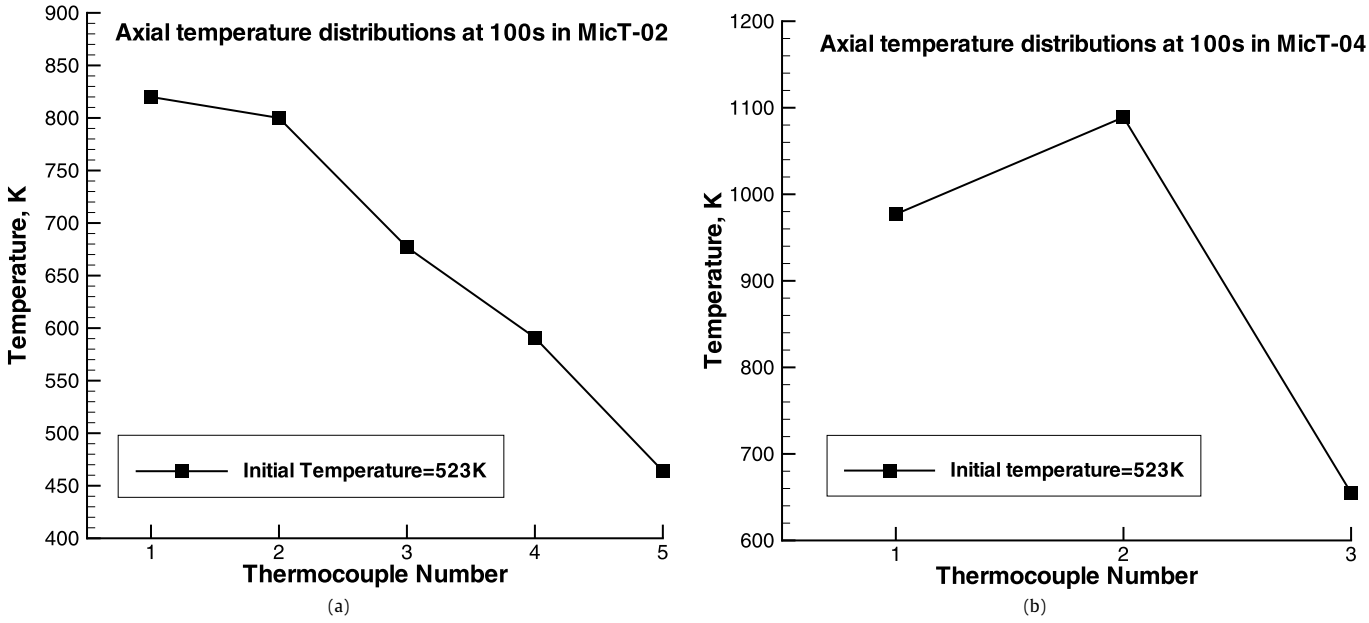

Fig. 11. (a) Axial temperature distribution in Mict02 at 100 s. (b) Axial temperature distribution in Mict04 at 100 s.

Table 5
Catalyst-bed used in the orthogonal experiments (M_f = mass flow rate, D_c = chamber diameter, L_c = catalyst bed length).

Reactor	M_f, g/s	D_c, mm	L_c, mm	Peak T, K
MicT-05	0.1	6	25	1278
MicT-06	0.1	8	35	1409
MicT-07	0.1	10	50	1171
MicT-08	0.55	6	35	1360
MicT-09	0.55	8	50	1373
MicT-10	0.55	10	25	1633
MicT-11	0.1	6	50	1168
MicT-12	0.1	8	25	1278
MicT-13	0.1	10	35	1347

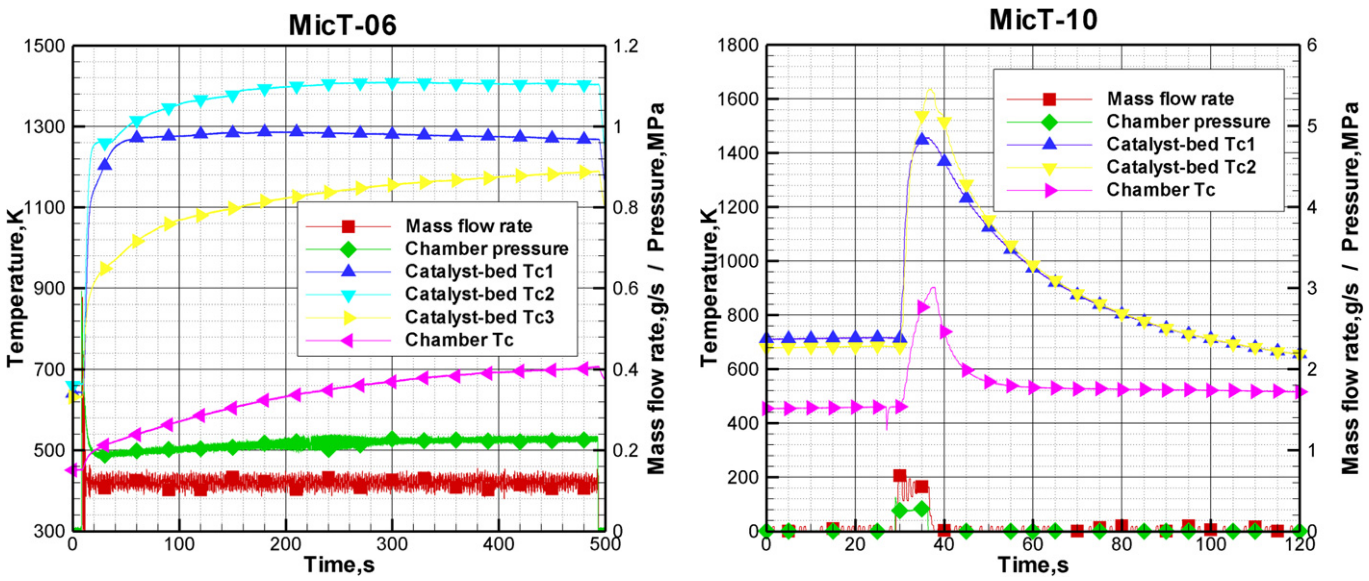

Fig. 12. (a) Experimental curves in Mict06. (b) Experimental curves in Mict10.

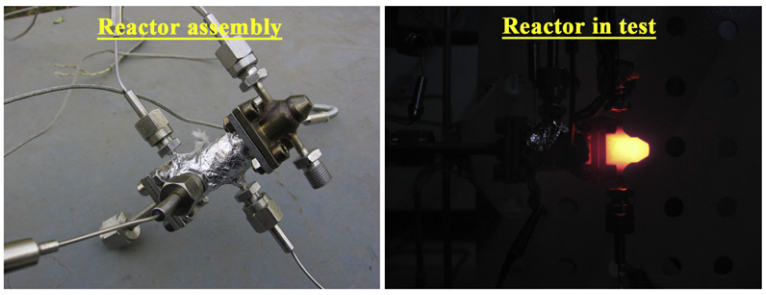

Fig. 13. Photograph of the reactor in orthogonal experiment.

rates, 0.1 g/s and 0.55 g/s, were employed in the experiments, in order to produce different thrusts within the sub-Newton range.

As shown in Table 5 and Fig. 12a, the peak catalyst-bed temperature at 0.1 g/s has surpassed 1400 K in a reactor with a Φ8 mm × 35 mm catalyst-bed (MicT-06), which was 300 K higher than the value of previous experiments at the same mass flow rate. A peak temperature of 1633 K or even higher, since it was the upper limit of the thermocouple, was achieved at a mass flow-rate of 0.55 g/s in a reactor with a Φ10 mm × 25 mm catalyst-bed (MicT-10). As shown in Fig. 12b, the reaction temperature in reactor MicT-10 increased rapidly, thus the control valve was shut down in a short time to protect the reactor and thermocouples. According to the reaction process of N_2O catalytic decomposition, there should be an optimum catalyst-bed for a specified mass flow rate. In an optimum catalyst-bed, most N_2O decomposes in the back region of the catalyst-bed and the temperature achieves the highest at the inlet of nozzle. If the catalyst-bed length is too short, the N_2O will not decompose completely. On the contrary, if it is too long, flow in the catalyst-bed will come into a "heat dissipation phase". Under either situation the energy of propellant will be wasted. Therefore, the configuration of the reactor MicT-10 is a good candidate since the temperature in the back region was higher than that in the front region. The reactor MicT-06 still has potential for further improvement.

The temperatures behind the catalyst-bed, named as chamber temperatures, were much lower than the temperatures measured in the catalyst-bed of the two reactors. This may be caused by large heat dissipation in this region. Since most of the N_2O had decomposed in the catalyst-bed, there was little N_2O decomposed behind the catalyst-bed. Therefore the heat dissipation rate was faster than the heat generation rate here. In addition, as shown in Fig. 13, there were many redundant structures in the back region of the reactor including the nozzle and the flanges for connecting the nozzle and the reaction chamber. They were all exposed to the outside circumstance in the experiments. This would reinforce the heat dissipation apparently. A photograph taken during a long-term experiment over 600 s is shown in Fig. 13. The stainless nozzle of the reactor was glowing bright yellow during the experiment. It indicated that there must be a lot of heat released from this part. If the redundant structures behind the reaction chamber were simplified and heat insulation measures were taken, the chamber temperature was expected to increase accordingly. Catalyst activity usually decreases during its operation because of poisoning, sintering, and attrition. The deterioration of catalyst is rapid at a high temperature. It was found that the temperature around 1400 K was a critical point for the current catalyst. When temperature exceeded this limit, the reactors were hard to be restarted. This might be a major limit to the performance improvement of the N_2O monopropellant thruster.

5.5. Assemblage and vacuum-thrust measuring for the thruster

A thruster was designed and fabricated based on the experimental results of N_2O catalytic decomposition. A Φ10 mm ×

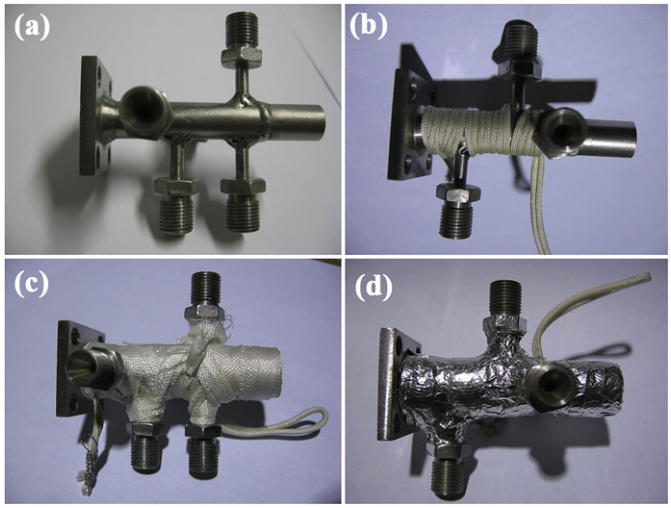

Fig. 14. Assembly of the heater and heat insulation layer.

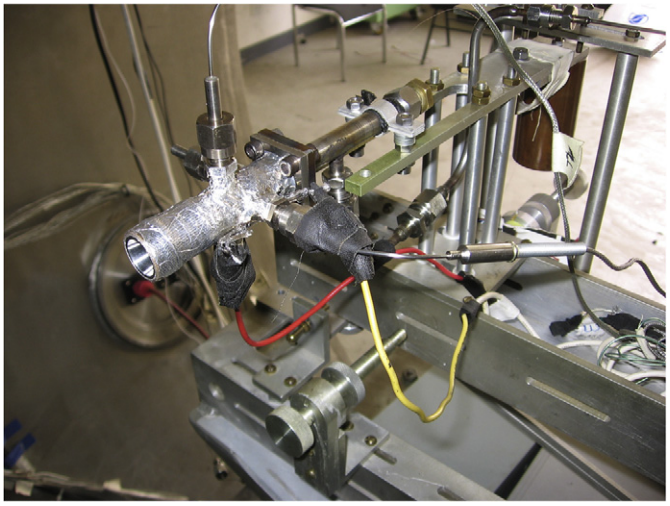

Fig. 15. Thruster fixed on the thrust-measuring stand.

25 mm catalyst-bed was employed due to its superior performance displayed in the catalyst-bed selection experiments. Iridium impregnated modified alumina catalyst with 17% metal content was employed in the thruster. Compared to the catalyst used in the previous experiments, there was a 10% reduction of the metal content. This measure was expected to prevent extreme temperature in the catalyst-bed and improve the thermal stability of the catalyst under high temperature. In addition, since it was found that the flanges used in the reactor for connecting the nozzle and the reaction chamber had resulted in larger amount of heat loss, further structure simplification was applied in the thruster by directly welding the two components together as illustrated in Fig. 14a. A conical nozzle with a 60° converging angle and 30° diverging angle was employed in the thruster. The throat diameter of the nozzle was 1.6 mm and the expansion ratio of the diverging section was 100. Catalyst grains with a characteristic dimension of around 0.9 mm were compactly loaded into the reaction chamber of the thruster to form the catalyst bed. Nickel-chrome wires were wrapped tightly around the reaction chamber as the preheating source (Fig. 14b). Outside these wires, several layers of glass fiber fabric were wrapped for heat insulation (Fig. 14c). Aluminum foil with a low surface emissivity was wrapped on the outermost layer (Fig. 14d), which may help to reduce the preheating energy as well as enhance the reaction temperature according to the simulation results on the preheating process.

As shown in Fig. 15, the vacuum-thrust measuring experiment was firstly conducted in the vacuum experimental system at a mass flow-rate of around 0.6 g/s. The experimental curves are shown in Fig. 16a. The catalyst-bed temperature in the thruster was below 1400 K, which was lower than the catalyst-bed temperature measured in the reactor MicT10. It demonstrated that the measure of using a catalyst with less metal content had successfully prevented the extreme reaction temperature in the thruster. The highest chamber temperature had reached 1380 K, which was much higher than the temperature measured in a reactor. It demonstrated that the structure simplification design and better heat insulation measures had brought significant performance enhancement for the thruster. The mean thrust at around 110 s had reached 973 mN, when the temperature and the thrust came into a quasi-stable phase. The corresponding specific impulse was about 1640 N s/kg. More thrust-measuring experiments were carried out in the same thruster with the mass flow rates altering from 0.5 g/s, 0.4 g/s, 0.3 g/s, 0.2 g/s, to 0.1 g/s, in order to review the performance of the thruster at different N_2O mass flow rates. The experimental curves are shown in Fig. 16b–f and a summary of the quasi-stable performances is shown in Fig. 17. By reducing the mass flow rate to around 0.1 g/s, the thrust can reach 140 mN at the lowest. It was found that the chamber temperature decreased along with the decrease of the N_2O mass flow rate, which in turn resulted in a gradual decrease of the specific impulse. Although the chamber temperatures were different, the catalyst-bed temperatures at a wide range of mass flow rates (from 0.2 g/s to 0.6 g/s) were similar. The chamber temperatures were lower than the catalyst-bed temperature when the mass flow rates were below 0.4 g/s. With the increase of the mass flow rate, the chamber temperature began to run after the catalyst-bed temperature and finally surpassed it. This reflected the influence of the catalyst-bed configuration on the thruster performance. As shown in Fig. 16a, when the catalyst-bed temperature reached around 1360 K, a slow decrease of the temperature occurred afterwards. This may result from the deterioration of catalyst at high temperature. Considering the high temperature performance of the current catalyst, the mass flow rate between 0.4–0.6 g/s was a suitable range for the current Φ10 mm × 25 mm catalyst-bed, because the catalyst-bed temperatures were close to the upper limit of the catalyst performance and the length of the catalyst-bed was effectively used. A specific impulse around 1600 N s/kg should be an applicable choice for the current thruster.

6. Conclusions

For an N_2O monopropellant thruster, more N_2O reactant decomposes in catalyst-bed will bring a higher reaction temperature and smaller mean molecular weight, which will help enhance specific impulse. Experiments of N_2O catalytic decomposition indicate that the loading factor and the length of catalyst-bed can influence the reaction effect of N_2O catalytic decomposition. Complete decomposition of N_2O reactant at a higher loading factor needs a longer distance in catalyst-bed. In order to achieve high specific impulse, structure optimization for catalyst-bed should be carried out for ensuring the temperature of reaction products reaches the highest at the inlet of the nozzle. In addition, heat absorption by thruster frame and heat dissipation from the outside-wall of the thruster shows negative effect on reaction temperature notably. In order to promote the efficient use of reaction heat so as to enhance the reaction temperature, heat insulation measures should be taken and the structure of the thruster should be simplified as much as possible. Tank pressure will decrease during N_2O self-

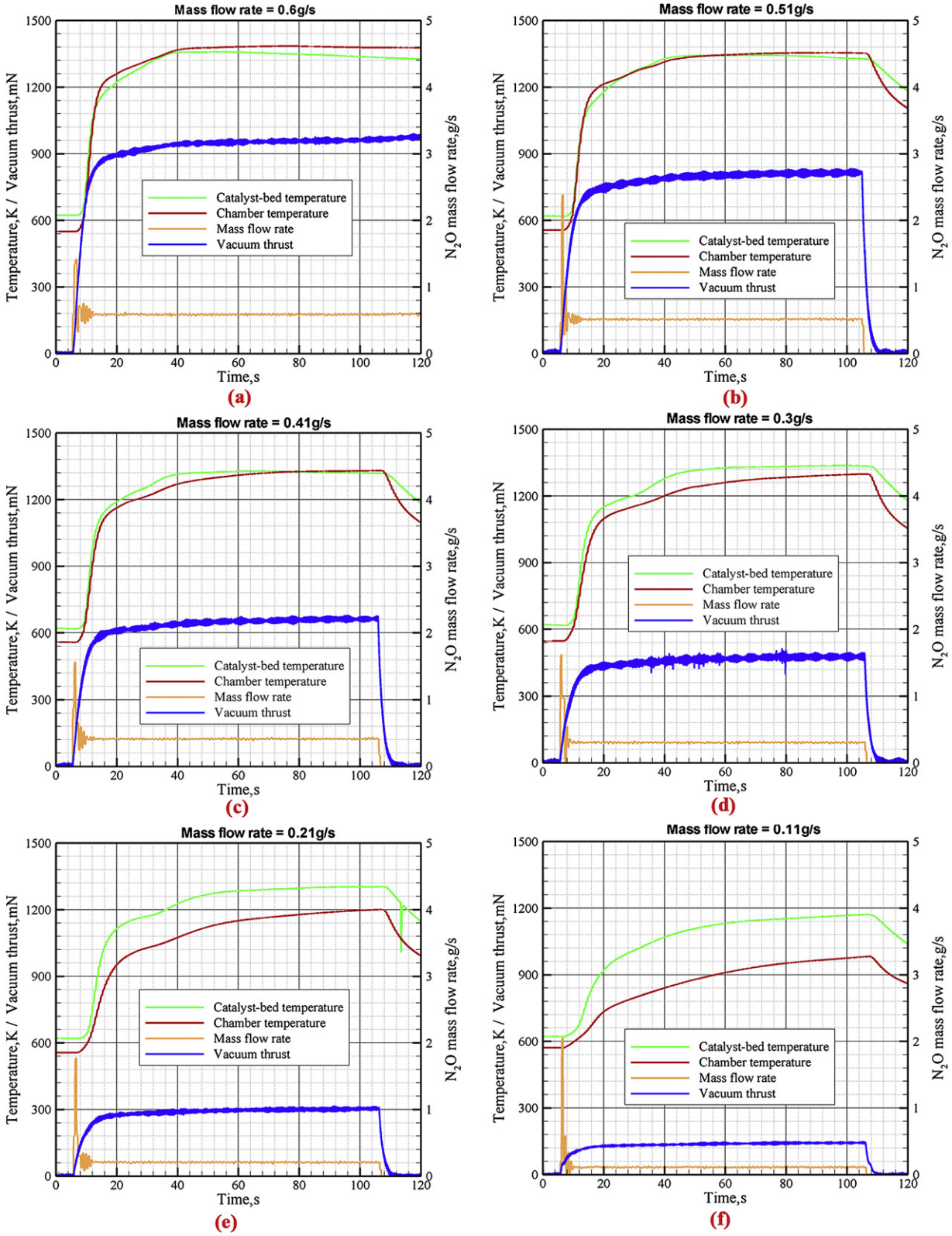

Fig. 16. Experimental results of vacuum-thrust measuring.

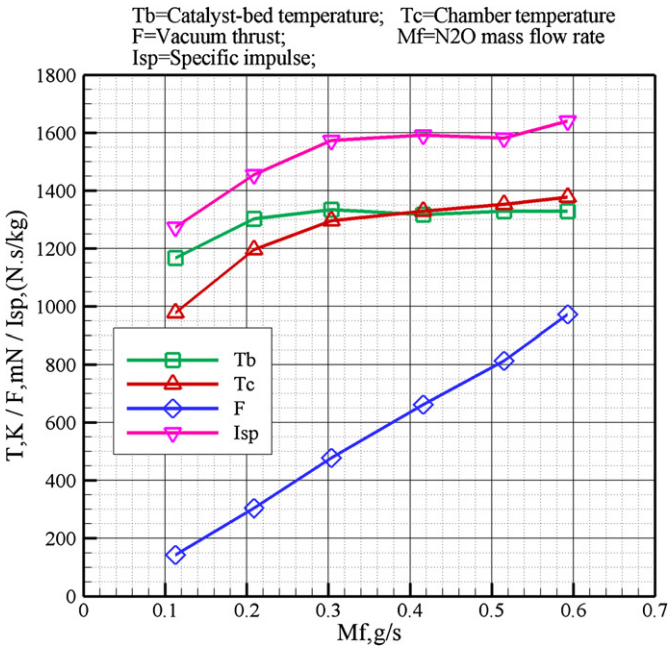

Fig. 17. Performance of the thruster at different mass flow rate.

pressurization process due to N_2O evaporation. Large pressure drop in late stage of tank self-pressurization process may influence the stability of N_2O flow rate. Simulated result indicates that reducing the surface emissivity is an effective method to improve the preheating performance, besides increasing the preheating power.

References

[1] J.P. Arves, J.H. Stephan, K. Kline, T. Bales, Development of a N2O-HTPB hybrid rocket motor, AIAA Paper 97-2803, 1997.

[2] J. Bristow, K. Hartman, A formation flying technology vision, AIAA Paper 2000-5194, 19–21 Sep. 2000.

[3] L. Casalino, D. Pastrone, Optimal design of hybrid rockets with self-pressurizing oxidizer, AIAA Paper 2006-4501, 9–12 July 2006.

[4] D. Gibbon, M. Paul, P. Jolley, V.A. Zakirov, G. Haag, I. Coxhill, M.N. Sweeting, R. Eloirdi, Energetic green propulsion for small spacecraft, AIAA Paper 2001-3247, 8–11 July 2001.

[5] W.A. Groot, S.R. Oleson, Chemical microthruster options, AIAA Paper 96-2868, 1–3 July 1996.

[6] F.S. Gulczinski, R.A. Spores, J. Stuhlberger, In-space propulsion, AIAA Paper 2003-2588, 14–17 July 2003.

[7] J. Huang (Ed.), Industrial Gas Data Book, Chemical Industry Press, Beijing, 2002, pp. 144–159.

[8] D.K. Huzel, D.H. Huang, Modern Engineering for Design of Liquid-Propellant Rocket Engines, American Institute of Aeronautics and Astronautics, Washington, DC, 2002 (Chapter 1).

[9] G.R. Jeffrey, J.S. Raymond, M.S. Manuel, Micropropulsion system selection for precision formation flying satellites, AIAA Paper 2001-3646, 8–11 July 2001.

[10] K. Lohner, J. Dyer, E. Doran, Z. Dunn, B. Krieger, V. Decker, E. Wooley, A. Sadhwani, B. Cantwell, T. Kenny, Design and development of a sub-scale nitrous oxide monopropellant gas generator, AIAA Paper 2007-5463, 8–11 July 2007.

[11] M. Martin, S. Kilberg, J. Winter, TechSat 21 and revolutionizing space missions using microsatellites, in: Proceedings of the 15th AIAA/USU Conference on Small Satellites, Logan, Utah, Aug. 2001, SSC01-1-3.

[12] M.M. Micci, A.D. Ketsdever, Micropropulsion for Small Spacecraft, Progress in Astronautics and Aeronautics, vol. 187, AIAA Press, Reston, VA, 2000.

[13] J. Mueller, Thruster options for microspacecraft: a review and evaluation of existing hardware and emerging technologies, AIAA Paper 97-3058, 1997.

[14] C. Norman, G. Tevfik, A review of micro propulsion technology, AIAA Paper 2003-670, 6–9 Jan. 2003.

[15] X. Roser, F. Arbusti, X. Leyre, M. Sghedoni, Formation flying enabling technologies for a big leap in science mission and perspectives for space projects, in: Proceedings of the 57th International Astronautical Congress, Valencia, Spain, 2–6 Oct. 2006, IAC-06-D1.4.05.

[16] Y. Scherson, K. Lohner, B. Lariviere, B. Cantwell, T. Kenny, A monopropellant gas generator based on N_2O decomposition for "green" propulsion and power applications, AIAA Paper 2009-4875, 2–5 August 2009.

[17] C. Tang, V.A. Zakirov, L. Li, Numerical simulation of liquefied gas self-pressurization for small spacecraft propulsion systems, Journal of Tsinghua University (Science & Technology) 47 (5) (2007) 730–733.

[18] N. Tiliakos, J.S. Tyll, R. Herdy, D. Sharp, M. Moser, N. Smith, Development and testing of a nitrous oxide/propane rocket engine, AIAA Paper 2001-3258, 8-11 July 2001.

[19] V. Zakirov, L. Li, Propulsion challenges for small spacecraft: 2005, Tsinghua Science and Technology 11 (24) (Oct. 2006) 507–514.

[20] V.A. Zakirov, M. Sweeting, An update on surrey nitrous oxide catalytic decomposition research, in: 15th AIAA/USU Conference on Small Satellites, Logan, Utah, Aug. 2001, SSC01-XI-2.

[21] V.A. Zakirov, H. Zhang, A model for the operation of nitrous oxide monopropellant, Aerospace Science and Technology 12 (4) (31 Aug. 2008) 318–323.

[22] V.A. Zakirov, V. Goeman, T.J. Lawrence, M.N. Sweeting, Surrey research on nitrous oxide catalytic decomposition for space applications, in: Proceedings of the 14th Annual AIAA/USC Conference on Small Satellites, Logan, Utah, Aug. 2000, SSC00-XI-6.

[23] V.A. Zakirov, G. Richardson, M. Sweeting, Surrey research update on N_2O catalytic decomposition for space applications, AIAA Paper 2001-3922, 2001.

[24] V.A. Zakirov, M.N. Sweeting, T.J. Lawrence, J.J. Sellers, Nitrous oxide as an rocket propellant, Acta Astronautica 48 (5–12) (2001) 353–362.

[25] V.A. Zakirov, Luming Li, Gong Ke, N_2O propulsion research at Tsinghua 2003, in: Proceedings of the 2nd International Conference on Green Propellants for Space Propulsion, Cagliari, Sardinia, Italy, June 2004.

[26] V.A. Zakirov, X.L. Huo, L. Li, Prospective N_2O monopropellant for future small satellite dual-mode propulsion, in: Proceedings of International Symposium on Space Propulsion 2004, Shanghai, PR China, August 25–28, 2004.

[27] X. Zhao (Ed.), Experimental Design Methods, Science Press, Beijing, 2006 (Chapter 4).

[28] G. Zilliac, M. Karabeyoglu, Modeling of propellant tank pressurization, AIAA Paper 2005-3549, 10–13 July 2005.